

# Visually Robust Adversarial Imitation Learning from Videos with Contrastive Learning

**Vittorio Giammarino**  
Division of Systems Engineering  
Boston University  
vgiammar@bu.edu

**James Queeney**  
Mitsubishi Electric Research Laboratories  
queeney@merl.com

**Ioannis Ch. Paschalidis**  
Department of Electrical and Computer Engineering  
Division of Systems Engineering  
Faculty of Computing & Data Sciences  
Boston University  
yannisp@bu.edu

**Abstract:** We propose C-LAIfo, a computationally efficient algorithm designed for imitation learning from videos, even in the presence of visual mismatch between agent and expert domains. We analyze the problem of imitation from expert videos with visual discrepancies, and introduce a solution for robust latent space estimation using contrastive learning and data augmentation. Provided a visually robust latent space, our algorithm performs imitation entirely within this space using off-policy adversarial imitation learning. We conduct a thorough ablation study to justify our design choices and test C-LAIfo on high-dimensional continuous robotic tasks. Additionally, we demonstrate how C-LAIfo can be combined with other reward signals to facilitate learning on a set of challenging hand manipulation tasks with sparse rewards. Our experiments show improved performance compared to baseline methods, highlighting the effectiveness and versatility of C-LAIfo. To ensure reproducibility, we provide open access to our [code](#).

## 1 Introduction

In recent years, there has been a significant surge in research on imitation learning from expert videos, commonly referred to as the *Visual Imitation from Observations (V-Ifo)* problem. The approach of mimicking experts from videos holds great promise for the future, as it offers a cost-effective way to teach autonomous agents new skills and behaviors. To achieve this goal, prior research has developed methods capable of concurrently addressing two primary challenges of the V-Ifo framework: the partial observability of the decision-making process and the absence of expert actions [1]. Despite these advancements, end-to-end state-of-the-art algorithms still face significant barriers in real-world applications due to the assumption that both the expert and learning agent operate within the same environment [1, 2]. For instance, consider the scenario described in Fig. 1, where expert videos are collected under the conditions in Fig. 1a and an autonomous agent is deployed in Fig. 1b or Fig. 1c. Current methods are not designed to handle such variations in lighting and background, leading to failures in these contexts. Our goal, in this paper, is to enhance the imitation capabilities of autonomous agents in the presence of visual mismatches.

In this context, our paper introduces a novel end-to-end pipeline for imitation from expert videos with visual mismatch. We begin by analyzing the V-Ifo problem with visual mismatch and propose a novel, simple, and computationally efficient algorithm called Contrastive Latent Adversarial Imitation from Observations (C-LAIfo). Notably, C-LAIfo builds upon the recent LAIfo algorithm [1] and achieves visually robust latent state estimation through data augmentation and contrastive learning techniques [3, 4]. We justify each design choice for our algorithm, including the types of data

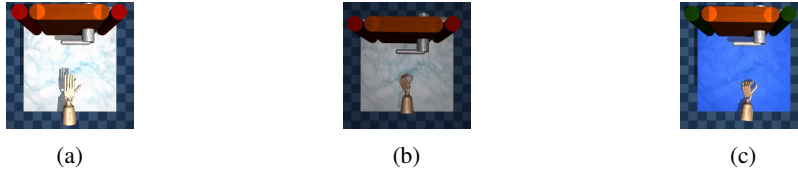


Figure 1: Robotic manipulation task. Current end-to-end methods for imitation from expert videos assume that the expert and the agent operate in the same environment. Consequently, they are unable to handle variations in lighting or background.

augmentation and contrastive loss, through a comprehensive ablation study. Furthermore, we evaluate the performance of C-LAIfo on the DeepMind Control Suite [5] and compare it against two V-IfO baselines—LAIfo [1] and PatchAIL [2]—as well as DisentanGAIL [6], which serves as a baseline for V-IfO with domain mismatch. Additionally, we show how the reward signal learned from expert data using C-LAIfo can be easily integrated with other signals to enhance efficiency and enable learning in scenarios with sparse rewards. In this context, we extend our algorithm’s evaluation to the Adroit platform for dynamic dexterous manipulation [7]. These additional experiments highlight the versatility of our approach, showcasing its efficacy in handling complex robotic tasks.

## 2 Related Work

Our work is closely related to the *Adversarial Imitation Learning (AIL)* framework [8], which has emerged as a promising approach to tackle the *Imitation Learning (IL)* problem. This framework builds upon a substantial body of research in inverse *Reinforcement Learning (RL)*, where the primary objective is to identify a reward function that enables expert demonstrations (state-action pairs) to be optimal [9, 10, 11, 12, 13, 14]. The derived reward function is then used to train RL agents capable of achieving expert-level performance.

AIL was initially formulated for the fully observable setting with access to expert actions [8, 15] and subsequently extended to observation-only scenarios in follow-up studies [16, 17, 18]. Furthermore, the stability and efficiency of this framework have been further investigated in [19, 20, 21, 22, 23]. In the context of partial observability, AIL has been explored for scenarios involving missing information [24], and in Visual IL where agents learn from video frames as state observations [25]. Relaxing the assumption on the availability of expert actions gives rise to the V-IfO problem, which is the primary focus of our work. State-of-the-art algorithms for the V-IfO setting include PatchAIL [2], which applies AIL directly on the pixel space utilizing a PatchGAN discriminator [26, 27], and LAIfo [1], where AIL operates on a latent representation of the agent state. Notably, these approaches are built on the assumption that both the expert and the learning agent act within the same decision process, which rarely holds true in real-world scenarios.

Our research focuses on the imitation problem from observations in the presence of domain mismatches between the expert and the learning agent. This framework is referred to in the literature under various names, including third-person IL [28], domain-adaptive IL [29], or cross-domain IL [30]. Previous solutions have approached this problem either by decomposing it into sequential stages [31] or using end-to-end methods. Among end-to-end approaches, some have addressed the fully observable setting [29, 32, 30, 33, 34], while others have tackled the visual (partially observable) setting [28, 35, 6, 36].

In the visual setting, [28] and [6] propose methods to extract domain-independent features useful for inferring a domain-independent reward function. The work in [28] learns domain-independent features using an adversarial approach similar to [37], while DisentanGAIL in [6] achieves a similar result by adding a mutual information constraint to the binary cross-entropy loss used for AIL. Similar to our algorithm, these studies formulate fully end-to-end model-free algorithms that avoid costly generative steps during the imitation process. Our approach adopts similar reasoning to [28, 6]; however, we leverage contrastive learning for domain-independent feature extraction and build the

entire AIL pipeline (both reward inference and RL step) on this learned feature space, rather than only the reward inference as done in [28, 6]. As shown in our experiments, this leads to significant improvements in performance.

In contrast, other works rely on expensive generative steps to address the mismatch problem. In [35], imitation is performed using expert observation-action pairs through a learned domain-agnostic recurrent state space model [38]. Our algorithm, on the other hand, is model-free and only requires expert observations. In [36], cycle-consistent adversarial networks [27] are used to generate expert videos in the agent’s domain, thus reducing the problem to the standard V-IfO without mismatches. Our approach does not require such a generative step, as it learns a domain-independent feature space directly.

### 3 Preliminaries

Unless indicated otherwise, we use uppercase letters (e.g.,  $S_t$ ) for random variables, lowercase letters (e.g.,  $s_t$ ) for values of random variables, script letters (e.g.,  $\mathcal{S}$ ) for sets, and bold lowercase letters (e.g.,  $\theta$ ) for vectors. Let  $[t_1 : t_2]$  be the set of integers  $t$  such that  $t_1 \leq t \leq t_2$ ; we write  $S_t$  such that  $t_1 \leq t \leq t_2$  as  $S_{t_1:t_2}$ . We denote with  $\mathbb{E}[\cdot]$  expectation, with  $\mathbb{P}(\cdot)$  probability, and with  $\mathbb{D}_f(\cdot, \cdot)$  an  $f$ -divergence between two distributions of which the Jensen-Shannon divergence,  $\mathbb{D}_{\text{JS}}(\cdot || \cdot)$ , is a special case.

**Partially Observable Markov Decision Process** We model the decision processes as infinite-horizon discounted Partially Observable Markov Decision Processes (POMDPs) described by the tuple  $(\mathcal{S}, \mathcal{A}, \mathcal{X}, \mathcal{T}, \mathcal{U}, \mathcal{R}, \rho_0, \gamma)$ , where  $\mathcal{S}$  is the set of states,  $\mathcal{A}$  is the set of actions, and  $\mathcal{X}$  is the set of observations.  $\mathcal{T} : \mathcal{S} \times \mathcal{A} \rightarrow P(\mathcal{S})$  is the transition probability function where  $P(\mathcal{S})$  denotes the space of probability distributions over  $\mathcal{S}$ ,  $\mathcal{U} : \mathcal{S} \rightarrow P(\mathcal{X})$  is the observation probability function, and  $\mathcal{R} : \mathcal{S} \times \mathcal{A} \rightarrow \mathbb{R}$  is the reward function which maps state-action pairs to scalar rewards. Finally,  $\rho_0 \in P(\mathcal{S})$  is the initial state distribution and  $\gamma \in [0, 1)$  the discount factor. The true environment state  $s \in \mathcal{S}$  is unobserved by the agent. Given an action  $a \in \mathcal{A}$ , the next state is sampled such that  $s' \sim \mathcal{T}(\cdot | s, a)$ , an observation is generated as  $x' \sim \mathcal{U}(\cdot | s')$ , and a reward  $\mathcal{R}(s, a)$  is computed. Note that an MDP is a special case of a POMDP where the underlying state  $s$  is directly observed.

**Reinforcement learning** Given an MDP and a stationary policy  $\pi : \mathcal{S} \rightarrow P(\mathcal{A})$ , the RL objective is to maximize the expected total discounted return  $J(\pi) = \mathbb{E}_\tau[\sum_{t=0}^{\infty} \gamma^t \mathcal{R}(s_t, a_t)]$  where  $\tau = (s_0, a_0, s_1, a_1, \dots)$ . A stationary policy  $\pi$  induces a normalized discounted state visitation distribution defined as  $d_\pi(s) = (1 - \gamma) \sum_{t=0}^{\infty} \gamma^t \mathbb{P}(s_t = s | \rho_0, \pi, \mathcal{T})$ , and we define the corresponding normalized discounted state-action visitation distribution as  $\rho_\pi(s, a) = d_\pi(s) \pi(a | s)$ . Finally, we denote the state value function of  $\pi$  as  $V^\pi(s) = \mathbb{E}_\tau[\sum_{t=0}^{\infty} \gamma^t \mathcal{R}(s_t, a_t) | S_0 = s]$  and the state-action value function as  $Q^\pi(s, a) = \mathbb{E}_\tau[\sum_{t=0}^{\infty} \gamma^t \mathcal{R}(s_t, a_t) | S_0 = s, A_0 = a]$ . When a function is parameterized with parameters  $\theta \in \Theta \subset \mathbb{R}^k$  we write  $\pi_\theta$ .

**Generative adversarial imitation learning** Assume we have a set of expert demonstrations  $\tau_E = (s_{0:T}, a_{0:T})$  generated by the expert policy  $\pi_E$ , a set of trajectories  $\tau_\theta$  generated by the policy  $\pi_\theta$ , and a discriminator network  $D_\chi : \mathcal{S} \times \mathcal{A} \rightarrow [0, 1]$  parameterized by  $\chi$ . Generative adversarial IL [8] optimizes the min-max objective

$$\min_{\theta} \max_{\chi} \mathbb{E}_{\tau_E} [\log(D_\chi(s, a))] + \mathbb{E}_{\tau_\theta} [\log(1 - D_\chi(s, a))]. \quad (1)$$

Maximizing (1) with respect to  $\chi$  is effectively an inverse RL step where a reward function,  $r_\chi(s, a) = -\log(1 - D_\chi(s, a))$ , is inferred by leveraging  $\tau_E$  and  $\tau_\theta$ . On the other hand, minimizing (1) with respect to  $\theta$  can be interpreted as an RL step, where the agent aims to minimize its expected cost. It has been demonstrated that optimizing the min-max objective in (1) is equivalent to minimizing  $\mathbb{D}_{\text{JS}}(\rho_{\pi_\theta}(s, a) || \rho_{\pi_E}(s, a))$ , so we are recovering the expert state-action visitation distribution [39].

**Modeling the visual mismatch in POMDPs** Traditionally, the V-IfO problem assumes that both the expert and the agent operate within the same POMDP. Throughout this paper we relax this assumption and define two different decision processes: namely a *target-POMDP* for the agent and a *source-POMDP* for the expert. The target-POMDP is characterized by the tuple  $(\mathcal{S}, \mathcal{A}, \mathcal{X}, \mathcal{T}, \mathcal{U}_T, \mathcal{R}, \rho_0, \gamma)$ ,

whereas the source-POMDP is characterized by the tuple  $(\mathcal{S}, \mathcal{A}, \mathcal{X}, \mathcal{T}, \mathcal{U}_S, \mathcal{R}, \rho_0, \gamma)$ . The primary distinction between these POMDPs lies in their observation probability functions. Despite sharing identical state and action spaces, given the same state  $s_t$ , the expert’s observation  $x_t^S \sim \mathcal{U}_S(\cdot|s_t)$  from the source-POMDP and the agent’s observation  $x_t^T \sim \mathcal{U}_T(\cdot|s_t)$  from the target-POMDP may be different (i.e., we may have  $x_t^S \neq x_t^T$ ). We refer to this as visual mismatch.

## 4 Contrastive Latent Adversarial Imitation from Observations

Considering a target-POMDP and a source-POMDP as introduced in the previous section, we can identify two levels of information in the observation space  $\mathcal{X}$ : (i) information related to task completion, and (ii) visual distractors that do not contribute to task completion. Thus, we define  $\mathcal{X}$  as  $\mathcal{X} = (\bar{\mathcal{X}}, \hat{\mathcal{X}})$ , where  $\bar{\mathcal{X}}$  represents the *goal-completion information* that is invariant between source-POMDP and target-POMDP; whereas,  $\hat{\mathcal{X}}$  represents the set of *visual distractors* that do not contribute to goal completion. We express the source and target observations respectively as  $x_t^S = (\bar{x}_t^S, \hat{x}_t^S)$  and  $x_t^T = (\bar{x}_t^T, \hat{x}_t^T)$ . Our objective is to filter out the visually-distracting information  $\hat{\mathcal{X}}$  from both the source and the target observations while retaining the goal-completion information  $\bar{\mathcal{X}}$  to effectively solve the V-IfO problem. This objective can be achieved by attaining *domain invariance in a feature space*  $\mathcal{Z}$ . As a result, our goal becomes to learn  $\mathcal{Z}$  such that only goal-completion information is retained while the visually-distracting information is discarded (cf. Appendix A for formal analysis).

In the following, we present the main components of our algorithm C-LAIfo, which performs imitation directly in a domain-invariant feature space  $\mathcal{Z}$ . In order to do so, we learn a domain-invariant encoder  $\phi_\delta$  that can successfully map  $x_{\leq t}^T$  and  $x_{\leq t}^S$  to  $z_t$  through two main steps. First, we train the encoder  $\phi_\delta$  alongside the critic networks  $Q_{\psi_k}$  where  $k = \{1, 2\}$ . This step is essential for solving the imitation problem and embedding goal-completion information within the latent space  $\mathcal{Z}$ . We further train  $\phi_\delta$  to optimize an auxiliary contrastive loss and perform randomized augmentation of the observations, taking into account the type of visual mismatch between the source and the target domains. This step is crucial to efficiently discard visually-distracting information from  $\mathcal{Z}$ .

**Adversarial imitation in latent space** Given a domain-invariant feature space  $\mathcal{Z}$ , our AIL pipeline is defined as follows. We initialize two replay buffers  $\mathcal{B}_E$  and  $\mathcal{B}$  to respectively store the sequences of observations generated by the expert and the agent policies, from which we infer the latent state-transitions  $(z_\delta, z'_\delta)$ . We write  $(z_\delta, z'_\delta) \sim \mathcal{B}$  to streamline the notation. Then, given a discriminator  $D_\chi : \mathcal{Z} \times \mathcal{Z} \rightarrow [0, 1]$ , we write

$$\max_{\chi} \mathbb{E}_{(z_\delta, z'_\delta) \sim \mathcal{B}_E} [\log(D_\chi(z_\delta, z'_\delta))] + \mathbb{E}_{(z_\delta, z'_\delta) \sim \mathcal{B}} [\log(1 - D_\chi(z_\delta, z'_\delta))]. \quad (2)$$

As mentioned, alternating (2) with an RL step using  $r_\chi(z_\delta, z'_\delta) = -\log(1 - D_\chi(z_\delta, z'_\delta))$  leads to the minimization of  $\mathbb{D}_{\text{JS}}(\rho_{\pi_\theta}(z_\delta, z'_\delta) || \rho_{\pi_E}(z_\delta, z'_\delta))$  [40]. Therefore, we are effectively imitating the expert in the latent space  $\mathcal{Z}$ . Note that the presented AIL can only succeed if  $\mathcal{Z}$  is domain-invariant and embeds the relevant goal-completion information necessary to solve the imitation problem. Next, we show how our algorithm C-LAIfo addresses this challenge.

**Critic and encoder training step** We define the encoder as  $\phi_\delta : \mathcal{X}^d \rightarrow \mathcal{Z}$ , a function mapping sequences of  $d \in \mathbb{N}$  observations to the latent space  $\mathcal{Z}$ . Specifically, we write  $z_\delta = \phi_\delta(x_{t^-:t})$  and  $z'_\delta = \phi_\delta(x_{t^-+1:t+1})$  where  $t - t^- + 1 = d$ . When a data augmentation function  $\text{aug}(\cdot)$  is applied to the sequence of observations, we write  $\tilde{z}_\delta = \phi_\delta(\text{aug}(x_{t^-:t}))$  and  $\tilde{z}'_\delta = \phi_\delta(\text{aug}(x_{t^-+1:t+1}))$ . We train  $\phi_\delta$  to optimize

$$\min_{\psi_k, \delta} \mathbb{E}_{(\tilde{z}_\delta, a_t, \tilde{z}'_\delta) \sim \mathcal{B}} [(Q_{\psi_k}(\tilde{z}_\delta, a_t) - \text{sg}(y))^2] + \mathbb{E}_{\tilde{z}_\delta \sim \mathcal{B}} [\mathcal{L}(\tilde{z}_\delta)] \quad (3)$$

$$\text{s.t. } y = r_\chi(z_\delta, z'_\delta) + \gamma \min_{k=1,2} Q_{\psi_k}(\tilde{z}'_\delta, a'). \quad (4)$$

The steps in (3)–(4) follow the deep  $Q$ -network optimization pipeline [41, 42], where we add a contrastive auxiliary loss  $\mathbb{E}_{\tilde{z}_\delta \sim \mathcal{B}} [\mathcal{L}(\tilde{z}_\delta)]$  in (3) defined on the encoder  $\phi_\delta$ . In (4), the reward function  $r_\chi(z_\delta, z'_\delta)$  is computed through the AIL step in (2). Note that we do not perform data augmentation

when computing  $r_{\mathcal{X}}$  since, during reward inference, we are deploying and not training the encoder  $\phi_{\delta}$ . In practice, adding data augmentation to AIL in (2) decreases the performance.

In (3), the encoder  $\phi_{\delta}$  is trained together with the critic networks  $Q_{\psi_k}$  ( $k = \{1, 2\}$ ) in order to regress  $y$  in (4), where  $\text{sg}(\cdot)$  stands for stop gradient of the encoder parameters  $\delta$ . The value of  $y$  in (4) is computed by summing  $r_{\mathcal{X}}$  with the discounted target critic network at time  $t + 1$ . In (4),  $a' = \pi_{\theta}(\tilde{z}'_{\delta}) + \epsilon$  where  $\epsilon \sim \text{clip}(\mathcal{N}(0, \sigma^2), -c, c)$  is a clipped exploration noise with  $c$  the clipping parameter and  $\mathcal{N}(0, \sigma^2)$  a univariate normal distribution with zero mean and  $\sigma$  standard deviation.  $\tilde{\psi}_1$  and  $\tilde{\psi}_2$  are the slow moving weights for the target critic networks.  $\mathcal{B}$  is a replay buffer initialized to store interactions  $(x_t^T, a_t, x_{t+1}^T)$  of the agent with the target environment. Note that the latent state-transitions  $(\tilde{z}_{\delta}, \tilde{z}'_{\delta})$  are inferred from sequences of observations using  $\phi_{\delta}$  and, as above, we write  $(\tilde{z}_{\delta}, \tilde{z}'_{\delta}) \sim \mathcal{B}$  to streamline the notation (cf. Appendix B for the complete pseudo-code).

By solving the optimization problem in (3)–(4), our primary goal is to train both the encoder network  $\phi_{\delta}$  and the critic networks  $Q_{\psi_k}$  to solve the RL problem with reward  $r_{\mathcal{X}}$ . In other words, this step focuses on retaining the goal-completion information within the latent space  $\mathcal{Z}$  such that critic networks  $Q_{\psi_k}$  are successfully learned. We show in our ablation study that backpropagating the gradient from  $Q_{\psi_k}$  to  $\phi_{\delta}$  is an important step for achieving this goal and solving the imitation problem. Similarly, the types of augmentations performed on the sequences of observations and the choice of auxiliary loss play a crucial role in discarding the visually-distracting information from  $\mathcal{Z}$  and dealing with the visual mismatch.

**Contrastive loss** In the following, we introduce the data augmentation techniques and the auxiliary loss  $\mathcal{L}$  in (3) for C-LAIfo. We opt for a contrastive method as this leads to good empirical results and good computational efficiency. Contrastive learning constructs low-dimensional representations of high-dimensional data by maximizing agreement between augmented views of the same data example via a contrastive loss in the latent space  $\mathcal{Z}$ . In our specific case, we define equivalent data as sequences of observations with the same goal-completion information. The data augmentation is randomized by considering a set of pre-determined functions. We will show in our experiments (Section 5) that both the choice of contrastive loss and the set of augmentation functions play an important role in filtering out visually-distracting information.

First, a stochastic data augmentation module transforms any given sequence of observations  $x_{t-.t}$  into two views, denoted  $\text{aug}(x_{t-.t})_i$  and  $\text{aug}(x_{t-.t})_j$ , which are denoted as the positive pairs. Note that two positive pairs must contain the same goal-completion information. Next, the encoder  $\phi_{\delta} : \mathcal{X}^d \rightarrow \mathcal{Z}$  extracts representation vectors from augmented sequences of observations. We write  $\tilde{z}_{\delta}(i) = \phi_{\delta}(\text{aug}(x_{t-.t})_i)$  and  $\tilde{z}_{\delta}(j) = \phi_{\delta}(\text{aug}(x_{t-.t})_j)$ . Finally, we apply the contrastive loss function

$$\mathcal{L}(z_{\delta}) = -\log \frac{\exp(\text{sim}(\tilde{z}_{\delta}(i), \tilde{z}_{\delta}(j))/\eta)}{\sum_{k=1}^{2N} \mathbb{1}_{[k \neq i]} \exp(\text{sim}(\tilde{z}_{\delta}(i), \tilde{z}_{\delta}(k))/\eta)}, \quad (5)$$

where  $\mathbb{1}_{[k \neq i]} \in \{0, 1\}$  is an indicator function equal to 1 if  $k \neq i$ ,  $\eta$  denotes a temperature parameter, and  $\text{sim}(\mathbf{u}, \mathbf{v}) = \mathbf{u}^T \mathbf{v} / \|\mathbf{u}\| \|\mathbf{v}\|$  denotes the cosine similarity. We sample a batch of  $N$  sequences of observations from the buffer  $\mathcal{B}$  and define pairs of augmented sequences derived from the batch, resulting in  $2N$  data points. The negative data points are not sampled explicitly. Instead, given a positive pair, we treat the other  $2(N - 1)$  augmented data points within the batch as negatives. Note that the loss in (5) is called the normalized temperature-scaled cross entropy loss or the Information Noise-Contrastive Estimation (InfoNCE) loss [43] and represents an upper bound of the negative mutual information between positive pairs. Therefore, by minimizing (5) as in (3) we are maximizing the mutual information between positive pairs in the latent space  $\mathcal{Z}$ .

## 5 Experiments

In this section, we present our experimental results. We begin with an ablation study to justify the key design choices of our algorithm. Next, we demonstrate how C-LAIfo effectively handles various types of visual mismatches in the V-Ifo setting. Finally, we showcase how C-LAIfo facilitates learning in challenging robotic manipulation tasks with sparse rewards and realistic visual inputs.

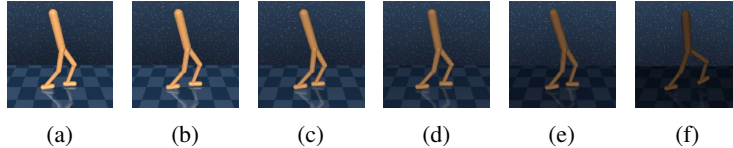


Figure 2: Different environments used for the ablation study in Table 1. The environment in (2a) represents the source-POMDP used to collect expert data, while (2b)–(2f) are different target-POMDPs. In these experiments, visual mismatch is introduced by varying the light intensity, with the degree of mismatch increasing linearly from (2b) to (2f).

Table 1: Summary of the ablation experiments. Refer to Fig. 2 for a visual representation of the different environments. We use DDPG [44] to train experts in a fully observable setting and collect 100 episodes of expert data. All algorithms are trained for  $10^6$  steps, and the learned policies are evaluated based on average return over 10 episodes. We report the mean and standard deviation of the final return over 6 seeds and **highlight** the best performance. The experiments *C-LAIfo w/o Q backprop*, *C-LAIfo full aug*, and *C-LAIfo w/o aug* are only conducted on the settings in (2b) and (2c) due to their low performance on these two easier settings.

Target Env	Source Env (2a), Performance = 950				
	(2b)	(2c)	(2d)	(2e)	(2f)
C-LAIfo	<b>936 ± 33.2</b>	<b>808 ± 269</b>	526 ± 334	<b>768 ± 231</b>	<b>895 ± 36.6</b>
BYOL-LAIfo	906 ± 76.1	707 ± 337	<b>696 ± 333</b>	142 ± 124	168 ± 139
C-LAIfo w/o Q backprop	114 ± 25.0	48.7 ± 8.7	-	-	-
C-LAIfo full aug	816 ± 209	96.8 ± 53.4	-	-	-
C-LAIfo w/o aug	641 ± 327	113 ± 25.3	-	-	-

**Ablation study** Given the environments in Fig. 2, we perform the following ablations:

1. **Contrastive loss function:** We demonstrate the importance of the contrastive loss function type by comparing the InfoNCE loss in (5) with BYOL in [4].
2. **Gradient backpropagation:** We highlight the necessity of backpropagating the gradient from  $Q_{\psi_k}$  to  $\phi_\delta$  in (3) for solving the imitation problem and embedding the goal-completion information in the latent space  $\mathcal{Z}$ .
3. **Data augmentation:** We emphasize the importance of selecting the appropriate augmentation for a given mismatch, showing that a mismatch-informed augmentation outperforms general augmentations or no augmentation.

The results of these experiments are summarized in Table 1, which includes results for C-LAIfo and its various configurations. All the learning curves are provided in Appendix D. In Table 1, *C-LAIfo* is implemented as described in Section 4, with the data augmentation function  $\text{aug}(\cdot)$  defined as a brightness transformation. In *BYOL-LAIfo*, we retain the design identical to C-LAIfo except for replacing the InfoNCE loss in (5) with BYOL [4]. In *C-LAIfo w/o Q backprop*, we disable gradient backpropagation from  $Q_{\psi_k}$  to  $\phi_\delta$  in (3). Lastly, in *C-LAIfo full aug* and *C-LAIfo w/o aug*, we respectively modify the data augmentation function  $\text{aug}(\cdot)$  to include full augmentation (brightness, color, and geometric transformations, as detailed in Appendix C) and no augmentation. Notably, without backpropagating the gradient from  $Q_{\psi_k}$  to  $\phi_\delta$ , C-LAIfo fails to solve the imitation task even in the simplest mismatch scenario in (2b). This result demonstrates the importance of this step for embedding goal-completion information in  $\mathcal{Z}$ . Conversely, without a well-designed  $\text{aug}(\cdot)$ , C-LAIfo can solve the imitation problem with minor visual mismatch but struggles with more challenging visual distractors. These results highlight the critical role of properly defining  $\text{aug}(\cdot)$  for efficient visual generalization in  $\mathcal{Z}$ . General  $\text{aug}(\cdot)$  might still achieve this goal, but much less efficiently. Finally, the superior performance of the InfoNCE loss in (5) compared to BYOL is particularly evident in handling the most difficult mismatches in (2e) and (2f).

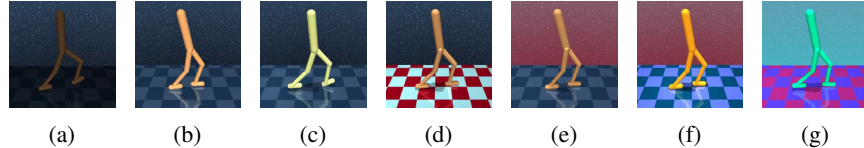


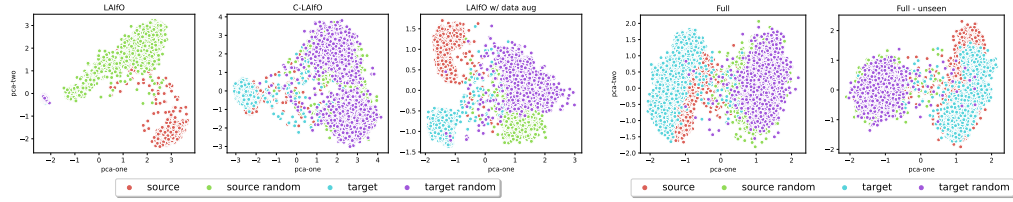
Figure 3: Different environments used for the experiments in Table 2 and the PCA in Fig. 4.

Table 2: Summary of the experiments for the mismatches in Fig. 3. The Light experiment consists in (3b) as source-POMDP and (3a) as target-POMDP. The Body, Floor, Background, and Full experiments have (3b) as target-POMDP and respectively (3c), (3d), (3e), and (3f) as source-POMDP. We use DDPG [44] to train experts in a fully observable setting and collect 100 episodes of expert data. We train all the algorithms for  $10^6$  steps, except for the Full mismatch, where we train for  $2 \times 10^6$  steps. We evaluate the learned policies based on the average return over 10 episodes. We report mean and standard deviation over 10 seeds and **highlight** the best performance.

	Light	Body	Floor	Background	Full
C-LAIfo	<b>895 ± 36.6</b>	<b>779 ± 199</b>	<b>486 ± 259</b>	<b>702 ± 164</b>	<b>509 ± 235</b>
LAIfo [1] w/ data aug	64.6 ± 62.9	714 ± 222	433 ± 304	315 ± 329	206 ± 210
DisentanGAIL [6]	28.1 ± 8.7	337 ± 215	75.6 ± 59.8	66.8 ± 53.9	30.6 ± 13.2
PatchAIL [2] w/ data aug	18.4 ± 5.6	597 ± 247	14.1 ± 2.4	29.9 ± 10.3	122 ± 66.6

**Visual Imitation from Observations with mismatch** In this section, we test C-LAIfo in the V-IfO setting with different types of mismatches (cf. Fig. 3) and compare it with three baselines: LAIfo [1] and PatchAIL [2], both equipped with the same  $\text{aug}(\cdot)$  used for C-LAIfo, and DisentanGAIL [6]. The results, summarized in Table 2, demonstrate that C-LAIfo successfully addresses the V-IfO with mismatch problem, achieving superior performance compared to all the baselines across the proposed mismatches. All the learning curves are provided in Appendix D. For the *Light* experiment,  $\text{aug}(\cdot)$  is defined as a brightness transformation; while for the others it is defined as a color transformation. Details on  $\text{aug}(\cdot)$  are provided in Appendix C. Furthermore, to assess whether C-LAIfo achieves *domain invariance in the feature space*  $\mathcal{Z}$ , we perform PCA and t-SNE analyses on the latent space  $\mathcal{Z}$  learned by different algorithms during training. Specifically, focusing on the *Light* experiment in Table 2, Fig. 4a compares the latent space  $\mathcal{Z}$  learned by LAIfo in [1], C-LAIfo, and LAIfo with data augmentation. Additionally, Fig. 4b investigates whether the latent space learned by C-LAIfo during the *Full* experiment can generalize to the unseen environment depicted in Fig. 3g. The results of this analysis are shown in Fig. 4, which includes the PCA visualization. For the t-SNE visualization and additional details refer to Appendix E.

**Improving RL using expert videos** In the following section, we examine a scenario where the reward  $r_{\chi}$  learned by C-LAIfo can be combined with a sparse reward  $\mathcal{R}$  that the agent collects through interaction with the environment. Consequently, the RL problem aims to maximize the total reward  $\mathcal{R}_{\text{tot}} = \mathcal{R}(s_t, a_t) + r_{\chi}(z_t, z_{t+1})$  with  $r_{\chi}$  learned through the AIL step in (2). We conduct experiments on the Adroit platform for dynamic dexterous manipulation [7] and compare C-LAIfo with DrQ-v2 [45], an RL-only baseline. In these experiments, both C-LAIfo and DrQ-v2 use an encoder to process pixel observations and extract embeddings in  $\mathcal{Z}$ , which are then concatenated with the robot sensory observations. Importantly, expert’s sensory observations are not used in the imitation problem as we only assume access to videos of experts. We denote our approach as RL+C-LAIfo since it maximizes  $\mathcal{R}_{\text{tot}}$  rather than only  $r_{\chi}$  alone as in the standard imitation learning problem. The results, summarized in Table 3, show that DrQ-v2 fails to learn in two out of three environments. In contrast, C-LAIfo successfully leverages expert videos with visual mismatch to facilitate learning. Note that the goal of these experiments is not merely to compare RL+C-LAIfo with DrQ-v2 but to demonstrate how C-LAIfo can leverage expert videos, even with visual mismatch, to enable learning in challenging robotic tasks. We provide all the learning curves in Appendix D.



(a) PCA results for the Light experiment in Table 2.

(b) PCA results on C-LAIfo for the Full experiment in Table 2 and the unseen environment in Fig. 3g.

Figure 4: In Fig. 4a we compare the latent space  $\mathcal{Z}$  learned by LAIfO, C-LAIfo, and LAIfO with data augmentation in the Light setting from Table 2. Specifically, we define *source* and *target* as the observations generated by an optimal policy in the source and target POMDPs, respectively. Similarly, *source random* and *target random* are observations generated by random policies. These observations are processed with the encoder  $\phi_\delta : \mathcal{X}^d \rightarrow \mathcal{Z}$  trained using the respective algorithms. We perform PCA on this set of latent variables  $z_{1:T}$  and plot the first two principal components. The results show that C-LAIfo is the only algorithm capable of filtering out visual distractors and clustering together data points with the same goal-completion information. In Fig. 4b, we focus on C-LAIfo and test for generalization to the unseen environment in Fig. 3g. We train  $\phi_\delta$  on the Full setting from Table 2 and perform PCA as described. The results in the unseen setting match those in the Full experiment, indicating that  $\phi_\delta$  trained on (3f) can successfully generalize to (3g).

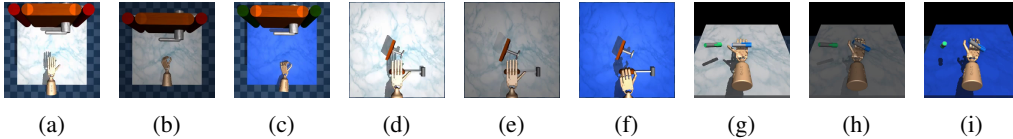


Figure 5: Adroit environments used for the experiments in Table 3.

Table 3: Summary of the experiments in Fig. 5. The Door-Light and Door-Color experiments consider (5a) as the source-POMDP and (5b) and (5c) as the respective target-POMDPs. Similarly, the Hammer-Light and Hammer-Color experiments consider (5d) as source-POMDP and (5e) and (5f) as the respective target-POMDPs, while the Pen-Light and Pen-Color experiments consider (5g) as source-POMDP and (5h) and (5i) as the respective target-POMDPs. We use the VRL3 pipeline in [46] to train expert policies and collect 100 episodes of expert data. All algorithms are trained for  $4 \times 10^6$  steps. We evaluate the learned policies based on the average return over 10 episodes. We report the mean and standard deviation over 10 seeds and **highlight** the best performance.

	Door		Hammer		Pen	
	Light	Color	Light	Color	Light	Color
Expert	170		184		73	
DrQ-v2 [45]	$-2.4 \pm 0.0$		$-1.8 \pm 2.2$		$53 \pm 9.0$	
RL+C-LAIfo	<b><math>106 \pm 75</math></b>	<b><math>96 \pm 80</math></b>	<b><math>181 \pm 4.0</math></b>	<b><math>103 \pm 86</math></b>	<b><math>59 \pm 12</math></b>	<b><math>59 \pm 4.8</math></b>

## 6 Conclusion

In this work, we analyze the V-IfO problem in the presence of visual mismatches and propose a novel algorithm named C-LAIfo as an effective solution. Through comprehensive ablation studies, we provide insights into our design choices and demonstrate the superior performance of our approach compared to a range of baselines in imitation from videos under various mismatch scenarios. Furthermore, we illustrate how C-LAIfo effectively utilizes expert videos with visual mismatches to facilitate learning in challenging hand manipulation tasks characterized by sparse rewards and realistic visual inputs.

**Limitations and future work** A main limitation of the current approach is given by the reliance of C-LAIfo on a well-designed, possibly mismatch-informed, data augmentation function. As illustrated in our ablations in Section 5, general augmentation can lead to poor performance or can remarkably reduce the algorithmic sample efficiency. Furthermore, it can be challenging to design effective augmentations for certain types of mismatches. To address this problem, exploring generative models for automatic data augmentation represents an interesting research direction. Generative models could produce diverse, mismatch-informed augmentations, potentially overcoming the limitations of manually designed strategies. Alternatively, investigating different auxiliary losses that are less reliant on augmentation techniques represents another interesting direction. Finally, future work will be devoted to go beyond simulated environments and test our algorithms on hardware in real-world scenarios.

## 7 Acknowledgements

Vittorio Giammarino and Ioannis Ch. Paschalidis were partially supported by the NSF under grants IIS-1914792, CCF-2200052, and ECCS-2317079, by the ONR under grant N00014-19-1-2571, by the DOE under grant DE-AC02-05CH11231, by the NIH under grant UL54 TR004130, and by Boston University. James Queeney was exclusively supported by Mitsubishi Electric Research Laboratories.

## References

- [1] V. Giammarino, J. Queeney, and I. Paschalidis. Adversarial imitation learning from visual observations using latent information. *Transactions on Machine Learning Research*, 2024. ISSN 2835-8856. URL <https://openreview.net/forum?id=ydPHjgf6h0>.
- [2] M. Liu, T. He, W. Zhang, Y. Shuicheng, and Z. Xu. Visual imitation learning with patch rewards. In *International Conference on Learning Representations*, 2022.
- [3] T. Chen, S. Kornblith, M. Norouzi, and G. Hinton. A simple framework for contrastive learning of visual representations. In *International Conference on Machine Learning*, pages 1597–1607. PMLR, 2020.
- [4] J.-B. Grill, F. Strub, F. Altché, C. Tallec, P. Richemond, E. Buchatskaya, C. Doersch, B. Avila Pires, Z. Guo, M. Gheshlaghi Azar, et al. Bootstrap your own latent—a new approach to self-supervised learning. *Advances in Neural Information Processing Systems*, 33: 21271–21284, 2020.
- [5] Y. Tassa, Y. Doron, A. Muldal, T. Erez, Y. Li, D. d. L. Casas, D. Budden, A. Abdolmaleki, J. Merel, A. Lefrancq, et al. Deepmind control suite. *arXiv preprint arXiv:1801.00690*, 2018.
- [6] E. Cetin and O. Celiktutan. Domain-robust visual imitation learning with mutual information constraints. In *International Conference on Learning Representations*, 2020.
- [7] V. Kumar. *Manipulators and Manipulation in high dimensional spaces*. PhD thesis, University of Washington, Seattle, 2016. URL <https://digital.lib.washington.edu/researchworks/handle/1773/38104>.

- [8] J. Ho and S. Ermon. Generative adversarial imitation learning. *Advances in Neural Information Processing Systems*, 29, 2016.
- [9] S. Russell. Learning agents for uncertain environments. In *Proceedings of the Annual Conference on Computational Learning Theory*, pages 101–103, 1998.
- [10] A. Y. Ng, S. Russell, et al. Algorithms for inverse reinforcement learning. In *International Conference on Machine Learning*, volume 1, page 2, 2000.
- [11] P. Abbeel and A. Y. Ng. Apprenticeship learning via inverse reinforcement learning. In *International Conference on Machine Learning*, page 1, 2004.
- [12] U. Syed and R. E. Schapire. A game-theoretic approach to apprenticeship learning. *Advances in Neural Information Processing Systems*, 20, 2007.
- [13] B. D. Ziebart, A. L. Maas, J. A. Bagnell, A. K. Dey, et al. Maximum entropy inverse reinforcement learning. In *AAAI Conference on Artificial Intelligence*, volume 8, pages 1433–1438. Chicago, IL, USA, 2008.
- [14] U. Syed, M. Bowling, and R. E. Schapire. Apprenticeship learning using linear programming. In *International Conference on Machine Learning*, pages 1032–1039, 2008.
- [15] J. Fu, K. Luo, and S. Levine. Learning robust rewards with adversarial inverse reinforcement learning. *arXiv preprint arXiv:1710.11248*, 2017.
- [16] F. Torabi, G. Warnell, and P. Stone. Generative adversarial imitation from observation. *arXiv preprint arXiv:1807.06158*, 2018.
- [17] C. Yang, X. Ma, W. Huang, F. Sun, H. Liu, J. Huang, and C. Gan. Imitation learning from observations by minimizing inverse dynamics disagreement. *Advances in Neural Information Processing Systems*, 32, 2019.
- [18] Z. Cheng, L. Liu, A. Liu, H. Sun, M. Fang, and D. Tao. On the guaranteed almost equivalence between imitation learning from observation and demonstration. *IEEE Transactions on Neural Networks and Learning Systems*, 2021.
- [19] I. Kostrikov, K. K. Agrawal, D. Dwibedi, S. Levine, and J. Tompson. Discriminator-actor-critic: Addressing sample inefficiency and reward bias in adversarial imitation learning. *arXiv preprint arXiv:1809.02925*, 2018.
- [20] L. Blondé and A. Kalousis. Sample-efficient imitation learning via generative adversarial nets. In *International Conference on Artificial Intelligence and Statistics*, pages 3138–3148. PMLR, 2019.
- [21] I. Kostrikov, O. Nachum, and J. Tompson. Imitation learning via off-policy distribution matching. *arXiv preprint arXiv:1912.05032*, 2019.
- [22] Z. Zhu, K. Lin, B. Dai, and J. Zhou. Off-policy imitation learning from observations. *Advances in Neural Information Processing Systems*, 33:12402–12413, 2020.
- [23] R. Kidambi, J. Chang, and W. Sun. Mobile: Model-based imitation learning from observation alone. *Advances in Neural Information Processing Systems*, 34:28598–28611, 2021.
- [24] T. Gangwani, J. Lehman, Q. Liu, and J. Peng. Learning belief representations for imitation learning in POMDPs. In *Uncertainty in Artificial Intelligence*, pages 1061–1071. PMLR, 2020.
- [25] R. Rafailov, T. Yu, A. Rajeswaran, and C. Finn. Visual adversarial imitation learning using variational models. *Advances in Neural Information Processing Systems*, 34:3016–3028, 2021.

- [26] P. Isola, J.-Y. Zhu, T. Zhou, and A. A. Efros. Image-to-image translation with conditional adversarial networks. In *Proceedings of the IEEE Conference on Computer Vision and Pattern Recognition*, pages 1125–1134, 2017.
- [27] J.-Y. Zhu, T. Park, P. Isola, and A. A. Efros. Unpaired image-to-image translation using cycle-consistent adversarial networks. In *Proceedings of the IEEE International Conference on Computer Vision*, pages 2223–2232, 2017.
- [28] B. C. Stadie, P. Abbeel, and I. Sutskever. Third-person imitation learning. *arXiv preprint arXiv:1703.01703*, 2017.
- [29] K. Kim, Y. Gu, J. Song, S. Zhao, and S. Ermon. Domain adaptive imitation learning. In *International Conference on Machine Learning*, pages 5286–5295. PMLR, 2020.
- [30] D. S. Raychaudhuri, S. Paul, J. Vanbaaar, and A. K. Roy-Chowdhury. Cross-domain imitation from observations. In *International Conference on Machine Learning*, pages 8902–8912. PMLR, 2021.
- [31] J. Z. Zhang, S. Yang, G. Yang, A. L. Bishop, S. Gurumurthy, D. Ramanan, and Z. Manchester. Slomo: A general system for legged robot motion imitation from casual videos. *IEEE Robotics and Automation Letters*, 2023.
- [32] A. Fickinger, S. Cohen, S. Russell, and B. Amos. Cross-domain imitation learning via optimal transport. In *International Conference on Learning Representations*, 2021.
- [33] T. Gangwani, Y. Zhou, and J. Peng. Imitation learning from observations under transition model disparity. *arXiv preprint arXiv:2204.11446*, 2022.
- [34] V. Giammarino, J. Queeney, L. C. Carstensen, M. E. Hasselmo, and I. C. Paschalidis. Opportunities and challenges from using animal videos in reinforcement learning for navigation. *IFAC-PapersOnLine*, 56(2):9056–9061, 2023.
- [35] R. Okumura, M. Okada, and T. Taniguchi. Domain-adversarial and-conditional state space model for imitation learning. In *2020 IEEE/RSJ International Conference on Intelligent Robots and Systems (IROS)*, pages 5179–5186. IEEE, 2020.
- [36] S. Choi, S. Han, W. Kim, J. Chae, W. Jung, and Y. Sung. Domain adaptive imitation learning with visual observation. In *Advances in Neural Information Processing Systems*, 2023.
- [37] Y. Ganin and V. Lempitsky. Unsupervised domain adaptation by backpropagation. In *International Conference on Machine Learning*, pages 1180–1189. PMLR, 2015.
- [38] D. Hafner, T. Lillicrap, I. Fischer, R. Villegas, D. Ha, H. Lee, and J. Davidson. Learning latent dynamics for planning from pixels. In *International Conference on Machine Learning*, pages 2555–2565. PMLR, 2019.
- [39] S. K. S. Ghasemipour, R. Zemel, and S. Gu. A divergence minimization perspective on imitation learning methods. In *Proceedings of the Conference on Robot Learning*, pages 1259–1277. PMLR, 2020.
- [40] I. Goodfellow, J. Pouget-Abadie, M. Mirza, B. Xu, D. Warde-Farley, S. Ozair, A. Courville, and Y. Bengio. Generative adversarial networks. *Communications of the ACM*, 63(11):139–144, 2020.
- [41] V. Mnih, K. Kavukcuoglu, D. Silver, A. Graves, I. Antonoglou, D. Wierstra, and M. Riedmiller. Playing atari with deep reinforcement learning. *arXiv preprint arXiv:1312.5602*, 2013.
- [42] V. Mnih, K. Kavukcuoglu, D. Silver, A. A. Rusu, J. Veness, M. G. Bellemare, A. Graves, M. Riedmiller, A. K. Fidjeland, G. Ostrovski, et al. Human-level control through deep reinforcement learning. *Nature*, 518(7540):529–533, 2015.

- [43] A. v. d. Oord, Y. Li, and O. Vinyals. Representation learning with contrastive predictive coding. *arXiv preprint arXiv:1807.03748*, 2018.
- [44] T. P. Lillicrap, J. J. Hunt, A. Pritzel, N. Heess, T. Erez, Y. Tassa, D. Silver, and D. Wierstra. Continuous control with deep reinforcement learning. *arXiv preprint arXiv:1509.02971*, 2015.
- [45] D. Yarats, R. Fergus, A. Lazaric, and L. Pinto. Mastering visual continuous control: Improved data-augmented reinforcement learning. *arXiv preprint arXiv:2107.09645*, 2021.
- [46] C. Wang, X. Luo, K. Ross, and D. Li. Vrl3: A data-driven framework for visual deep reinforcement learning. *Advances in Neural Information Processing Systems*, 35:32974–32988, 2022.

## A Analysis

In the following, we show how *domain invariance in the feature space*  $\mathcal{Z}$  leads to the same V-IfO guarantees as in [1], even in the presence of visual mismatches.

**Proposition 1.** *Consider source and target POMDPs respectively defined by the tuples  $(\mathcal{S}, \mathcal{A}, \mathcal{X}, \mathcal{T}, \mathcal{U}_T, \mathcal{R}, \rho_0, \gamma)$  and  $(\mathcal{S}, \mathcal{A}, \mathcal{X}, \mathcal{T}, \mathcal{U}_S, \mathcal{R}, \rho_0, \gamma)$ . Let  $\mathcal{X} = (\bar{\mathcal{X}}, \hat{\mathcal{X}})$ , where  $\bar{\mathcal{X}}$  is an observations set invariant between source and target POMDP, and  $\hat{\mathcal{X}}$  is a set of visual distractors. We write  $x_t = (\bar{x}_t, \hat{x}_t)$ . Assume  $z_t = \phi(x_{\leq t}) = \phi(\bar{x}_{\leq t})$  such that  $\mathbb{P}(s_t|z_t, a_t) = \mathbb{P}(s_t|z_t) = \mathbb{P}(s_t|x_{\leq t}, a_{<t}) = \mathbb{P}(s_t|\bar{x}_{\leq t}, a_{<t})$ . Then, the filtering posterior distributions  $\mathbb{P}(s_t|z_t)$  and  $\mathbb{P}(s_{t+1}, s_t|z_{t+1}, z_t)$  do not depend on the policy  $\pi$  and are invariant between source and target POMDPs.*

*Proof.* Considering the definition of the latent variable  $z_t$ , which only depends on  $\bar{x}_{\leq t}$  and not the visually-distracting information  $\hat{x}_{\leq t}$ , we can write

$$\mathbb{P}(s_t|z_t) = \mathbb{P}(s_t|x_t, a_{t-1}, z_{t-1}) = \mathbb{P}(s_t|\bar{x}_t, a_{t-1}, z_{t-1}).$$

Then, by leveraging Bayes rule we have that

$$\begin{aligned} \mathbb{P}(s_t|z_t) &= \mathbb{P}(s_t|\bar{x}_t, a_{t-1}, z_{t-1}) \\ &= \frac{\mathbb{P}(\bar{x}_t|s_t, a_{t-1}, z_{t-1})\mathbb{P}(s_t|a_{t-1}, z_{t-1})}{\mathbb{P}(\bar{x}_t|a_{t-1}, z_{t-1})} \\ &= \frac{\mathbb{P}(\bar{x}_t|s_t) \int_{\mathcal{S}} \mathcal{T}(s_t|s_{t-1}, a_{t-1})\mathbb{P}(s_{t-1}|z_{t-1})ds_{t-1}}{\int_{\mathcal{S}} \int_{\mathcal{S}} \mathbb{P}(\bar{x}_t|s_t)\mathcal{T}(s_t|s_{t-1}, a_{t-1})\mathbb{P}(s_{t-1}|z_{t-1})ds_t ds_{t-1}}, \end{aligned}$$

where the denominator can be seen as a normalizing factor. Note that  $\mathbb{P}(\bar{x}_t|s_t)$  is the same for both the source and target POMDPs by the definition of  $\bar{\mathcal{X}}$  above. Therefore,  $\mathbb{P}(s_t|z_t)$  has no dependence on the policy  $\pi$  and is invariant between source and target POMDP.

Similarly, for  $\mathbb{P}(s_{t+1}, s_t|z_t, z_{t+1})$  we have that

$$\begin{aligned} \mathbb{P}(s_{t+1}, s_t|z_t, z_{t+1}) &= \mathbb{P}(s_t, s_{t+1}|\bar{x}_{t+1}, a_t, z_t) \\ &= \frac{\mathbb{P}(\bar{x}_{t+1}|s_t, s_{t+1}, a_t, z_t)\mathbb{P}(s_t, s_{t+1}|a_t, z_t)}{\mathbb{P}(\bar{x}_{t+1}|a_t, z_t)} \\ &= \frac{\mathbb{P}(\bar{x}_{t+1}|s_{t+1})\mathcal{T}(s_{t+1}|s_t, a_t)\mathbb{P}(s_t|z_t)}{\int_{\mathcal{S}} \int_{\mathcal{S}} \mathbb{P}(\bar{x}_{t+1}|s_{t+1})\mathcal{T}(s_{t+1}|s_t, a_t)\mathbb{P}(s_t|z_t)ds_{t+1} ds_t}. \end{aligned}$$

Because  $\mathbb{P}(s_t|z_t)$  does not depend on  $\pi$  and is the same for both source and target POMDP, the result also holds for  $\mathbb{P}(s_{t+1}, s_t|z_t, z_{t+1})$ .  $\square$

**Proposition 2.** *Given  $\mathcal{R} : \mathcal{S} \times \mathcal{A} \rightarrow \mathbb{R}$ , for the scenarios described in Proposition 1 the following inequality holds:*

$$|J(\pi_E) - J(\pi_\theta)| \leq \frac{2R_{\max}}{1-\gamma} \mathbb{D}_{\text{TV}}(\rho_{\pi_\theta}(z, z'), \rho_{\pi_E}(z, z')) + C,$$

where  $R_{\max} = \max_{(s,a) \in \mathcal{S} \times \mathcal{A}} |\mathcal{R}(s, a)|$  and

$$C = \frac{2R_{\max}}{1-\gamma} \mathbb{E}_{\rho_{\pi_\theta}(z, z')} [\mathbb{D}_{\text{TV}}(\mathbb{P}_{\pi_\theta}(a|z, z'), \mathbb{P}_{\pi_E}(a|z, z'))]. \quad (6)$$

If  $\mathcal{R} : \mathcal{S} \times \mathcal{S} \rightarrow \mathbb{R}$ , then we have that

$$|J(\pi_E) - J(\pi_\theta)| \leq \frac{2R_{\max}}{1-\gamma} \mathbb{D}_{\text{TV}}(\rho_{\pi_\theta}(z, z'), \rho_{\pi_E}(z, z')),$$

where  $R_{\max} = \max_{(s,s') \in \mathcal{S} \times \mathcal{S}} |\mathcal{R}(s, s')|$ .

*Proof.* Because Proposition 1 holds, we can directly follow the proofs of Theorem 1 and Theorem 2 in [1] for the setting of no visual mismatch.  $\square$

## B Pseudo-code and hyperparameters

---

### Algorithm 1: C-LAIfo

---

**Inputs:**

Expert observations:  $(x_n^S)_{0:N} \in \mathcal{B}_E$ .

$\pi_\theta, D_\chi, Q_{\psi_1}, Q_{\psi_2}, \phi_\delta$ : networks for policy, discriminator, Q functions and encoder.

$T_{\text{train}}, \sigma(t), d, \text{aug}, c, \tau, B, \alpha, \alpha_D, \gamma, \eta$ : training steps, scheduled standard deviation, frames stack dimension, stochastic data augmentation, clip value, target update rate, batch size, learning rate, discriminator learning rate, discount factor and temperature parameter.

**for**  $t = 1, \dots, T_{\text{train}}$  **do**

$\sigma_t \leftarrow \sigma(t)$

**if**  $t \geq d - 1$  **then**

$z_t \leftarrow \phi_\delta(x_{t-d+1:t}^T)$

**else**

$z_t \leftarrow \phi_\delta(x_{0:t}^T)$

$a_t \leftarrow \pi_\theta(z_t) + \epsilon$  and  $\epsilon \sim \mathcal{N}(0, \sigma_t^2)$

$s_{t+1} \sim \mathcal{T}(\cdot | s_t, a_t)$  and  $x_{t+1} \sim \mathcal{U}_T(\cdot | s_{t+1})$

$\mathcal{B} \leftarrow \mathcal{B} \cup (x_t^T, a_t, x_{t+1}^T)$

    UpdateEncoder( $\mathcal{B}$ )

    UpdateDiscriminator( $\mathcal{B}, \mathcal{B}_E$ )

    UpdateCritic( $\mathcal{B}$ )

    UpdateActor( $\mathcal{B}$ )

**begin** UpdateEncoder

$\{(x_{t-d+1:t}^T, a_t, x_{t-d+2:t+1}^T)\} \sim \mathcal{B}$  (sample  $B$  transitions)

$\tilde{z}_\delta(i) \leftarrow \phi_\delta(\text{aug}(x_{t-d+1:t}^T)_i)$  and  $\tilde{z}_\delta(j) \leftarrow \phi_\delta(\text{aug}(x_{t-d+1:t}^T)_j)$

    Update  $\phi_\delta$  to minimize (5) with learning rate  $\alpha$

**begin** UpdateDiscriminator

$\{(x_{t-d+1:t}^S, x_{t-d+2:t+1}^S)\} \sim \mathcal{B}_E$  and  $\{(x_{t-d+1:t}^T, x_{t-d+2:t+1}^T)\} \sim \mathcal{B}$  (sample  $B$  transitions)

$z_\delta \leftarrow \phi_\delta(x_{t-d+1:t}^T)$  and  $z'_\delta \leftarrow \phi_\delta(x_{t-d+2:t+1}^T)$  for both agent and expert

    Update  $D_\chi$  to minimize BCE loss with learning rate  $\alpha_D$

**begin** UpdateCritic

$\{(x_{t-d+1:t}^T, a_t, x_{t-d+2:t+1}^T)\} \sim \mathcal{B}$  (sample  $B$  transitions)

$\tilde{z}_\delta \leftarrow \phi_\delta(\text{aug}(x_{t-d+1:t}^T))$  and  $\tilde{z}'_\delta \leftarrow \phi_\delta(\text{aug}(x_{t-d+2:t+1}^T))$

$a_{t+1} \leftarrow \pi_\theta(\tilde{z}_\delta) + \epsilon$  and  $\epsilon \sim \text{clip}(\mathcal{N}(0, \sigma_t^2), -c, c)$

    Update  $Q_{\psi_1}, Q_{\psi_2}$  and  $\phi_\delta$  to minimize (3) with  $r_\chi(z_\delta, z'_\delta)$  and learning rate  $\alpha$

$\tilde{\psi}_k \leftarrow (1 - \tau)\tilde{\psi}_k + \tau\psi_k \quad \forall k \in \{1, 2\}$

**begin** UpdateActor

$\{x_{t-d+1:t}^T\} \sim \mathcal{B}$  (sample  $B$  observations)

$\tilde{z}_\delta \leftarrow \phi_\delta(\text{aug}(x_{t-d+1:t}^T))$

$a_t \leftarrow \pi_\theta(\tilde{z}_\delta) + \epsilon$  and  $\epsilon \sim \text{clip}(\mathcal{N}(0, \sigma_t^2), -c, c)$

    Update  $\pi_\theta$  using DDPG [44] with learning rate  $\alpha$

---

Table 4: Hyperparameter values for C-LAIfo experiments.

Hyperparameter Name	Value
Frames stack ( $d$ )	3
Discount factor ( $\gamma$ )	0.99
Image size	$64 \times 64$
Batch size ( $B$ )	256
Optimizer	Adam
Learning rate ( $\alpha$ )	$10^{-4}$
Discriminator learning rate ( $\alpha_D$ )	$4 \times 10^{-4}$
Target update rate ( $\tau$ )	0.01
Clip value ( $c$ )	0.3
Temperature parameter ( $\eta$ )	1.0

## C Data augmentation

The operations used in our data augmentation functions for the experiments in Section 5 are summarized in Table 5. Fig. 6 shows an example of color augmentation as implemented for the experiments in Table 2, where we randomly perform all the operations in the color transformations row in Table 5. On the other hand, Fig. 7 shows only a brightness transformation as implemented in the ablation study in Table. 1. Full augmentation in Table 1 performs all the operations in Table 5. For additional details refer to our [code](#)<sup>1</sup>.

Table 5: Operations used in our data augmentation function.

	Operations
Color transformations	Brightness Contrast Saturation Hue Grayscale Gaussian blur Invert
Affine transformations	Horizontal flip Vertical flip Resized crop

<sup>1</sup><https://github.com/VittorioGiammarino/C-LAIfo>

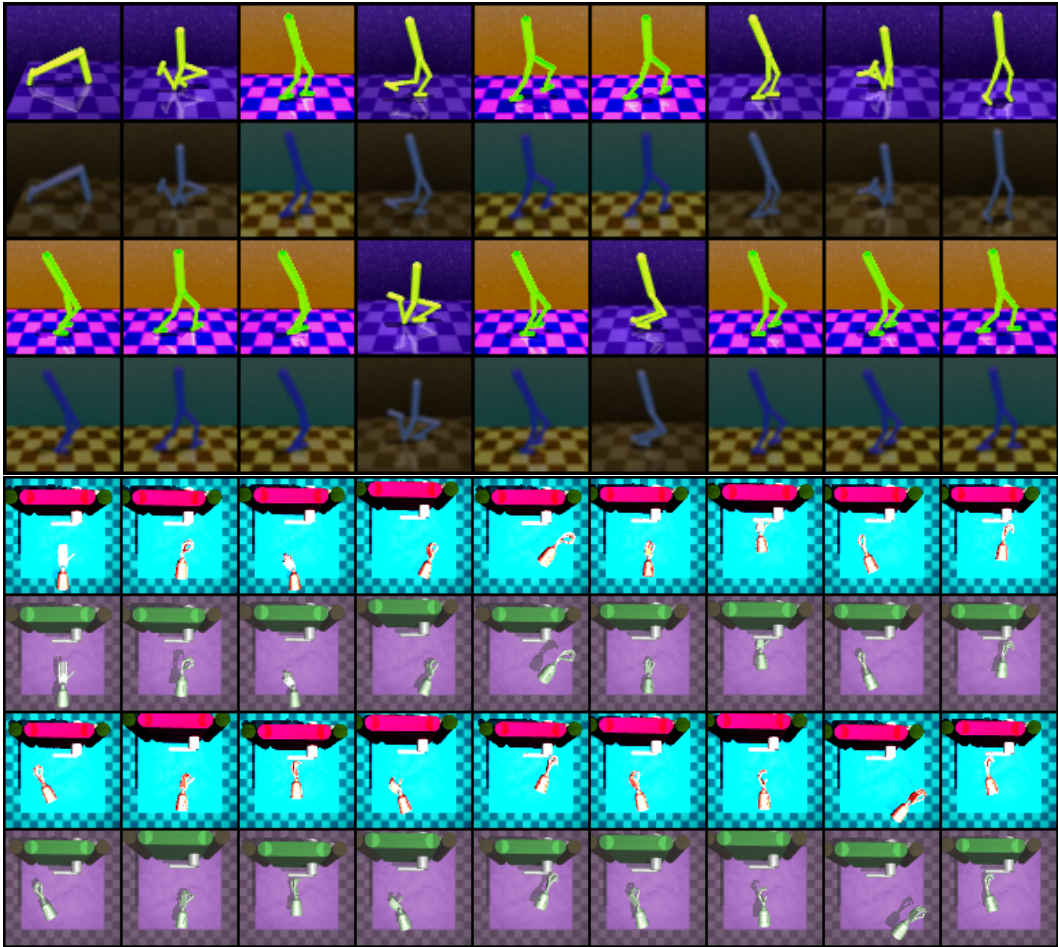


Figure 6: Examples of augmentation as color transformation.



Figure 7: Examples of augmentation as brightness transformation.

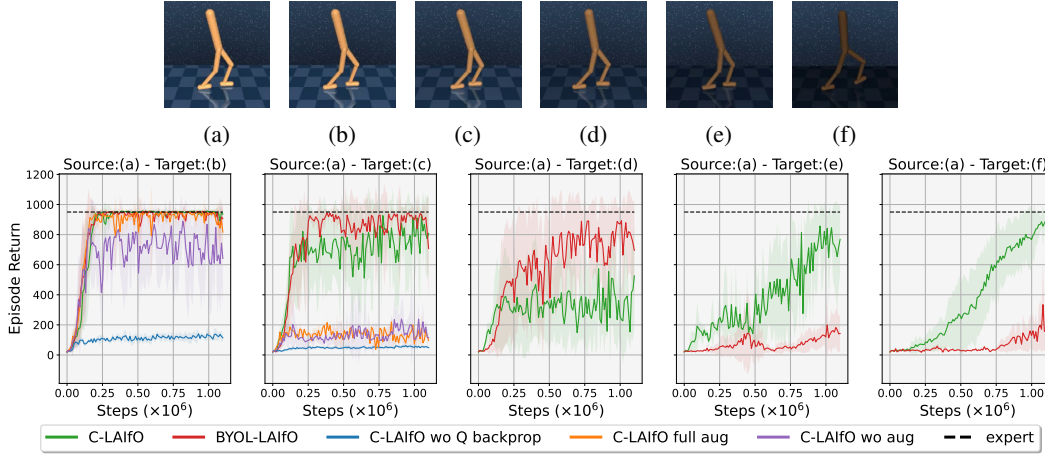


Figure 8: Learning curves for the results in Table 1. Plots show the average return per episode as a function of training steps. The environment in (8a) represents the source-POMDP used to collect expert data, while (8b)–(8f) are different target-POMDPs. In these experiments, visual mismatch is introduced by varying the light intensity, with the degree of mismatch increasing linearly from (8b) to (8f).

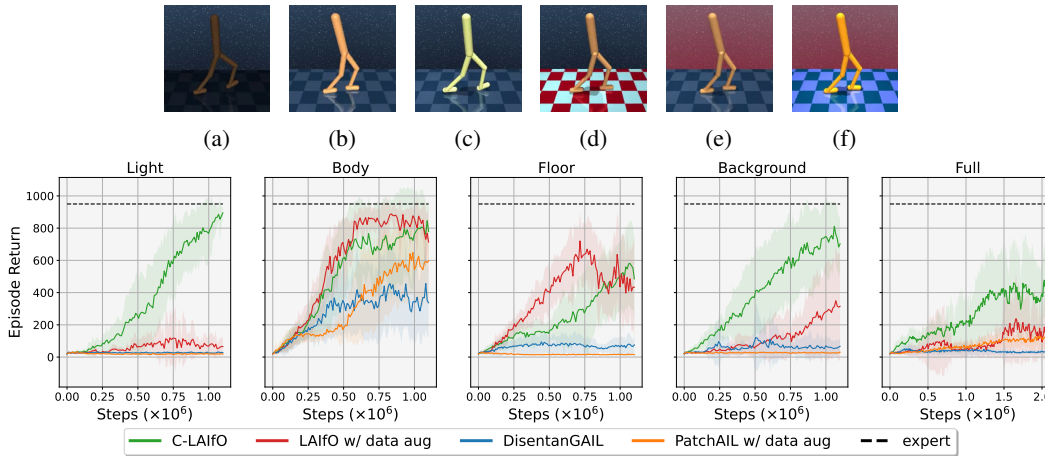


Figure 9: Learning curves for the results in Table 2. Plots show the average return per episode as a function of training steps. The Light experiment consists in (9b) as source-POMDP and (9a) as target-POMDP. The Body, Floor, Background, and Full experiments have (9b) as target-POMDP and respectively (9c), (9d), (9e), and (9f) as source-POMDP.

## D Learning curves

All the experiments are run using Nvidia-A40 GPUs on an internal cluster. For each algorithm, we run two experiments in parallel on the same GPU and each experiment takes 1 to 4 days depending on the simulated environment and the considered algorithm. For all the implementation details refer to our [code](#).

Fig. 8, Fig. 9, and Fig. 10 show the learning curves for the results in Table 1, Table 2, and Table 3, respectively.

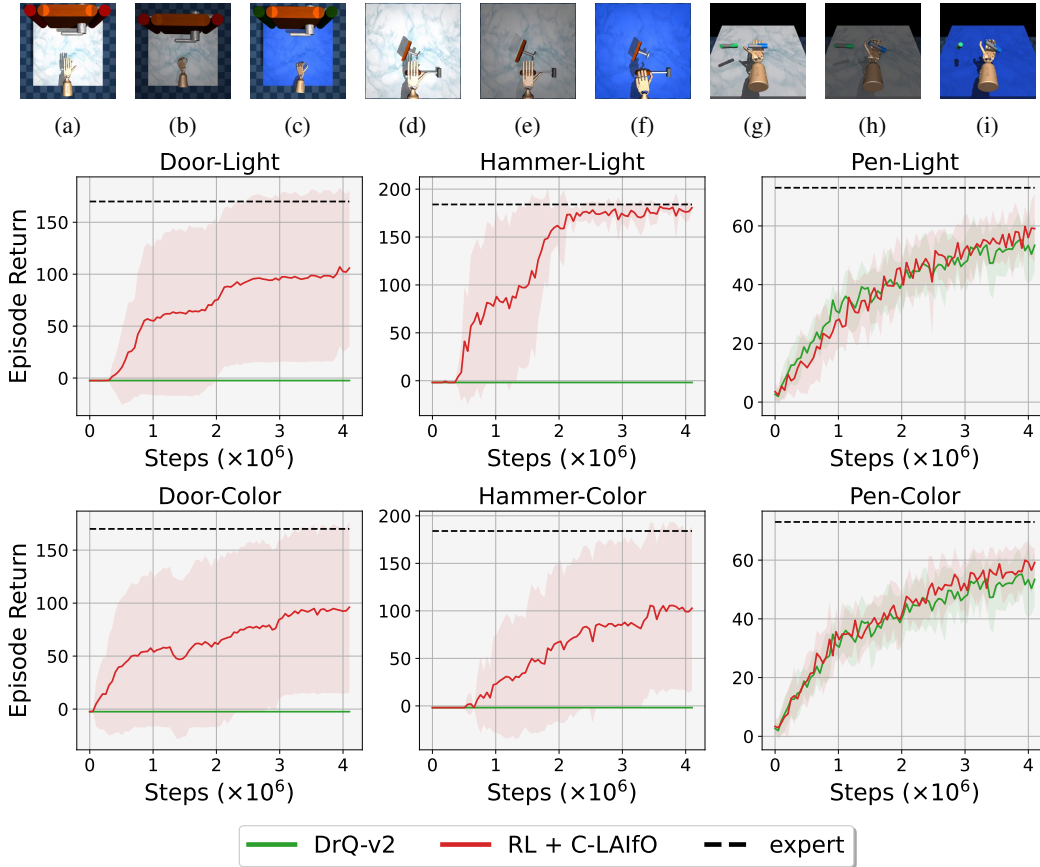


Figure 10: Learning curves for the results in Table 3. Plots show the average return per episode as a function of training steps. The Door-Light and Door-Color experiments consider (10a) as the source-POMDP and (10b) and (10c) as the respective target-POMDPs. Similarly, the Hammer-Light and Hammer-Color experiments consider (10d) as source-POMDP and (10e) and (10f) as the respective target-POMDPs, while the Pen-Light and Pen-Color experiments consider (10g) as source-POMDP and (10h) and (10i) as the respective target-POMDPs.

## E PCA and t-SNE analysis

In Fig. 11 we compare the latent space  $\mathcal{Z}$  learned by LAIfO, C-LAIfO, and LAIfO with data augmentation in the Light setting from Table 2 and Fig. 8. Specifically, we define *source* and *target* as the observations generated by an optimal policy in the source and target POMDPs, respectively. Similarly, *source random* and *target random* are observations generated by random policies. These observations are processed with the encoder  $\phi_\delta : \mathcal{X}^d \rightarrow \mathcal{Z}$  trained using the respective algorithms. We perform PCA and t-SNE on this set of latent variables  $z_{1:T}$  and plot the first two principal components. The results show that C-LAIfO is the only algorithm capable of filtering out visual distractors and clustering together data points with the same goal-completion information. In Fig. 12, we focus on C-LAIfO and test for generalization to the unseen environment in Fig. 12c. We train  $\phi_\delta$  on the Full setting from Table 2 and Fig. 9 and perform PCA and t-SNE as described. In Fig. 12, the Full figures have (12a)-(12b) as source-POMDP and (12e)-(12f) as target-POMDP. Similarly the Full-unseen figures have (12c)-(12d) as source-POMDP and (12e)-(12f) as target-POMDP. The results in the Full-unseen setting match those in the Full experiment, indicating that  $\phi_\delta$  trained on (12a) can successfully generalize to (12c).

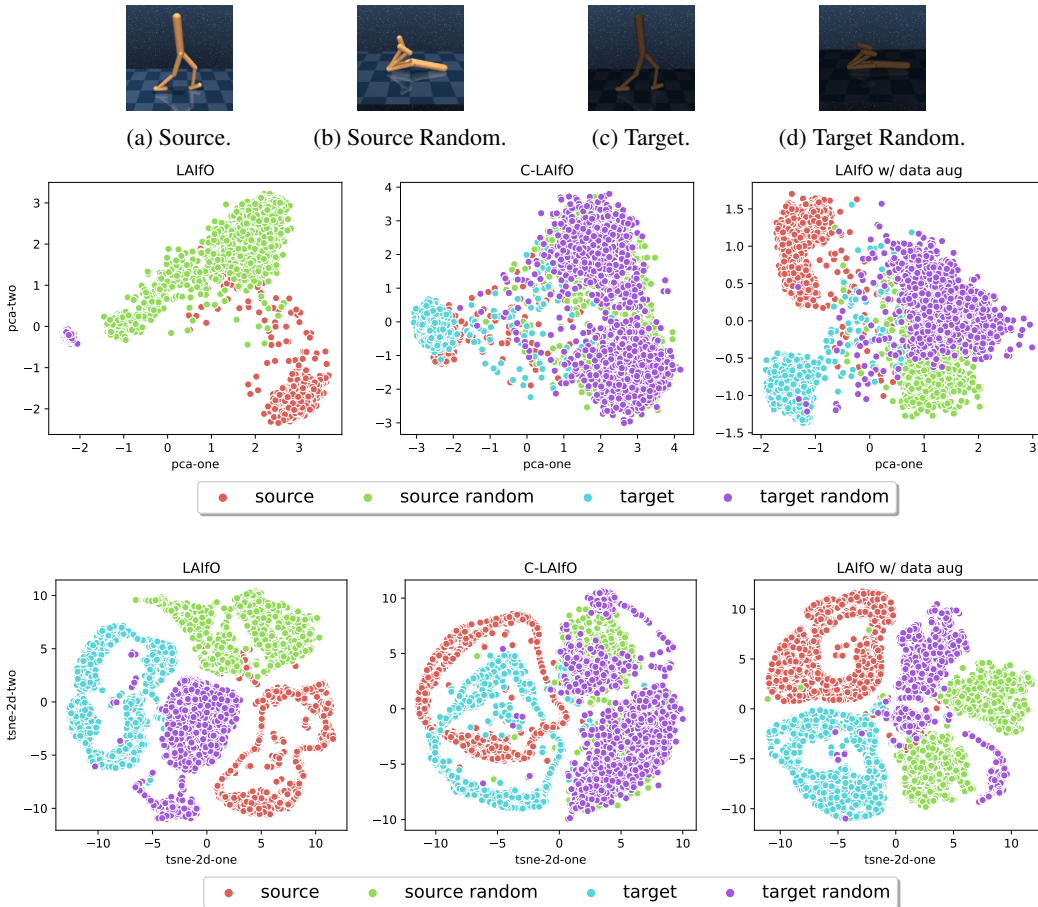


Figure 11: PCA and t-SNE visualizations for the Light experiment in Table 2.

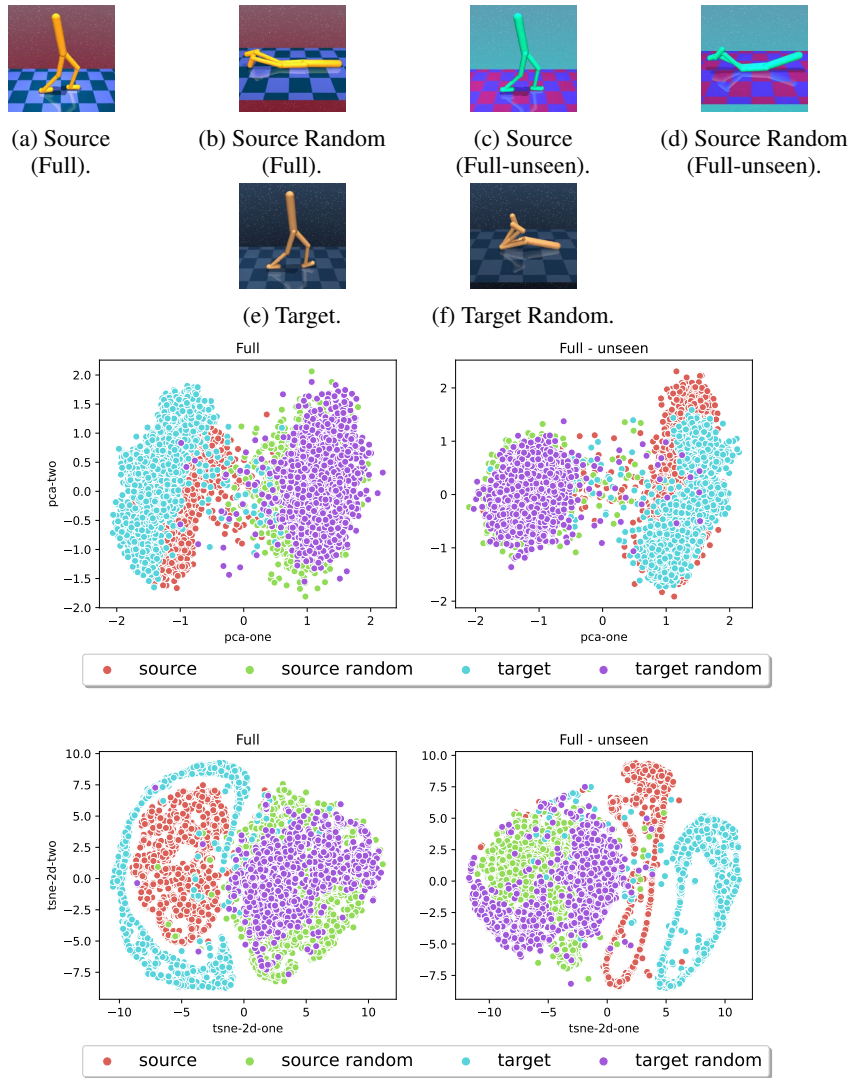


Figure 12: PCA and t-SNE for the Full experiment in Table 2. Fig. 12a and Fig. 12b denote the source environment for the Full experiment (left figures in Fig. 12). Fig. 12c and Fig. 12d denote the source environment for the Full-unseen experiment (right figures in Fig. 12).